RSC Advances

ROYAL SOCIETY OF CHEMISTRY

www.rsc.org/advances

Cite this: DOI: 10.1039/c0xx00000x

www.rsc.org/xxxxxx

PAPER

Quantum Tunneling of Magnetization in GaN:Mn nanoparticles

Yongsheng Xu[1] , Binbin Yao[1*], Qiliang Cui[2*]

Received (in XXX, XXX) Xth XXXXXXXXX 20XX, Accepted Xth XXXXXXXXX 20XX
DOI: 10.1039/b000000x

The GaN:Mn nanoparticles were synthesized successfully by DC arc discharge plasma without any catalyst or template. X-ray diffraction patterns revealed that all peaks position of GaN:Mn nanoparticles were shifted towards larger angles, indicating the c lattice parameter of GaN:Mn is smaller than that of GaN due to the lattice distortion. The growth mechanism explains the characteristic of morphology and size. Room temperature photoluminescence (PL) of GaN:Mn nanostructure exhibits a relatively broad range of visible light absorption due to dopant-induced energy levels within the band gap increasing the yield for electron-hole pair formation under illumination with visible light. The magnetic property was investigated by VSM and Quantum Design MPMS SQUID. Mn doped GaN nanoparticles show two prominent critical points corresponding to the magnetic phase transition, respectively. One is the classical thermally driven from superparamagnetic (SP) to blocked SP, the other is the quantum tunneling of magnetization from magnetic long-range order to quantum superparamagnetic (QSP) atate. The magnetism is derived from the Mn atoms, the magnetic coupling between Mn atoms depends on the mediating of N.

Introduction

The diluted magnetic semiconductors (DMSs) are crucial in spintronics - spin based electronics which utilize both the semiconducting and magnetic properties of one material,[1-4] thus a great attention has been devoted for preparation and study.[5-7] DMSs are semiconductors doped with transition metals or rare earth exhibiting magnetic properties. And the appropriate doping is to improve their performance in both electronic and optoelectronic devices.[8] Doped nanoparticles of dimensions below Bohr excition radius exhibit interesting optoelectronic and magnetic properties due to remarkable quantum size effect and the three-dimensional quantum confinement of electrons and holes.[9,10] The most interesting aspects of magnetic materials in modern times is that the observation of unusual properties derived from macroscopic quantum tunneling of magnetization (QTMs), which has continued to attract widespread attention.[11] Below a certain "critical size", ferromagnetic material exhibit a single domain in contrast to the usual multidomain structure of bulk materials behaving the interesting superparamagnetic (SP), which may have important consequences in determining the lifetime of magnetic information stroage.[12,13] However, the SP disappears when the thermal fluctuation of the random spin orientation is freeze. The SP state is transfer to a long-range magnetic order. If the size is ultrasmall, the Quantum tunneling of magnetization (QTM) take place as temperature further decreases, the superparamagnetic state can be re-observe even when the thermal energy is smaller than the barrier height.[11] It is denoted as quantum superparamagnetic (QSP), which offers a very exciting possibility for computers using mesoscopic magnets for memory.[14] To date, some effort has been put into study the Quantum tunneling of magnetization (QTM).

GaN is well-known for its excellent optoelectronic properties with direct and wide bandgap, high electron mobility, and excellent thermal stability.[15,16] It is one of the perspective materials for the field of spintronics, which is based on the control of the spin. In the recent years, the synthesis, characterization, and application of GaN DMSs nanostructures such as nanotubes,[17] nanorods,[18] and nanowires[19, 20] have attracted considerable attention because of that the properties of nanomaterials may have strong dependence on their size, morphology, and shape.[21, 22] Some GaN DMSs (doped Cr, Mn, Mg) nanostructures have been synthesized by various methods.[23-25] Some transition metal doped GaN materials exhibit the room temperature ferromagnetic ordering[26-28] and paramagnetism.[29,30] To our knowledge, Mn doped GaN nanoparticles with the quantum superparamagnetic have not yet been reported in literature. It is natural to draw the attention to GaN:Mn nanoparticles and to study their properties.

In this work, a simple, one-step, catalyst- and template-free method has been used the synthesis of Mn doped GaN nanoparticles; there is a chemical-vapor transport and condensation process in DC arc discharge plasma. The structure, morphology, size, optical and magnetic properties of GaN:Mn nanoparticles have been analyzed by X-ray diffraction (XRD), X-ray photoelectron spectroscopy (XPS), high resolution transmission electron microscopy (HRTEM), photoluminescence spectroscopy (PL), vibrating sample magnetometer (VSM) and Quantum Design MPMS SQUID. The optical and magnetic mechanisms have been investigated in detail. And the characterization of magnetism reveals that the GaN:Mn nanoparticles show two magnetic phase transition processes.

Experimental

The synthesis of Mn doped GaN nanoparticles were carried out in an improved DC arc discharge plasma setup. High-purity Mn (purity 99.99%) and Ga_2O_3 (purity 99.99%) were mixed and used as target raw materials. NH_3 (purity 99.999%) gas and N_2 gas (purity 99.999%) were used as nitrogen sources. The mixing column was used as both the evaporation source and deposition substrate. Before the DC arc was ignited, the chamber was evacuated to less than 5 pa of pressure, and then N_2 gas and NH_3 gas were introduced into the chamber at a pressure of 40 kPa. When the DC arc was ignited, the input current was maintained at 100 A and the voltage was a little higher than 25 V. The process of the GaN:Mn nanoparticles formation in the device involves the evaporation of Mn and Ga_2O_3, decomposition of NH_3 and N_2, nucleation of GaN, and instead of Ga. In the process, Ga_2O_3 plays a key role in the growth of GaN cryatal, as an oxide-assisted growth. The reaction time and the N_2 pressure is controlled accurately in order to the growth of the sphere-shaped nanostructure of GaN:Mn. After about 5 min of reaction, the substrate was covered with a larger number of samples. Finally, the products were passivated for about 24 h in pure Ar gas at 50 kPa.

The crystal structure and composition of GaN:Mn were characterized by the powder X-ray diffraction (XRD) patterns of using a Rigaku D/Max-A diffractometer with Cu Kα radiation, and X-ray photoelectron spectroscopy (XPS) using ESCALAB MK II. The morphology and microstructure were recorded by a field emission scanning electron microscopy (SEM) using XL 30 ESEM FEG, and a transmission electron microscopy (TEM) and a high resolution transmission electron microscopy (HRTEM) using a JEOL 2100 TEM operated at 200 kV and point to point resolution of 0.14 nm. The photoluminescence spectrum was measured with a sapphire laser as excitation source. The magnetic properties were measured using a vibrating sample magnetometer (VSM) and Quantum Design MPMS SQUID.

Results and Discussions

After the synthesis, the yellow powder was collected. The crystal structure of the products was examined by X-ray diffraction (XRD) measurements. Fig. 1 shows the X-ray diffraction patterns of GaN and GaN:Mn sample. The diffraction peaks are assigned to be hexagonal GaN phase according to the JCPDS Cards (JCPDS card No. 50-0792) except the asterisk. The XRD data confirms that Mn ions were incorporated in GaN to form GaN:Mn without changing the hexagonal structure. But all peaks position of the GaN:Mn shifted slightly toward larger angle (lower d value), indicating the c lattice parameter of GaN:Mn ($C_{GaN:Mn}$ =0.5129 nm) is smaller than that of GaN (C_{GaN} = 0.5184 nm).[31] Thaler et al. also showed a decrease in c lattice parameter at low Mn concentration.[32] It is suggested that the GaN:Mn has been synthesized, and the substitution of Mn ions can lead to lattice distortion. The ionic radius of Mn is only slightly smaller than that of Ga, and the Ga positions can be easily substituted by Mn under certain conditions, so Mn as dopant is more effective in practice than using other dopants.[8] This same phenomemon has been observed in others studies.[33-35] It implies that Mn ions are atomically doped inside the GaN:Mn nanostructure. The dopant content of sample was 4% and 7% measured by EDS testing, the sample can be written as $Ga_{0.96}Mn_{0.04}N$ and $Ga_{0.93}Mn_{0.07}N$. Furthermore, the asterisk is assigned to be O_2 coming from the intermediate product, which should be chemisorbed on the surface. As shown in Fig. 1, the O_2 peak of GaN:Mn is stronger than that of pure GaN. It indicates that the surface of GaN:Mn adsorbs more oxygen. As everyone knows that dopant-induced lowering of the vacancy formation energy of substituted ions can cause a substantial surface restructuring.[36] Here, the Mn doping increased surface defects and expanded surface uneven force field, which can seriously affect chemisorbed oxygen.

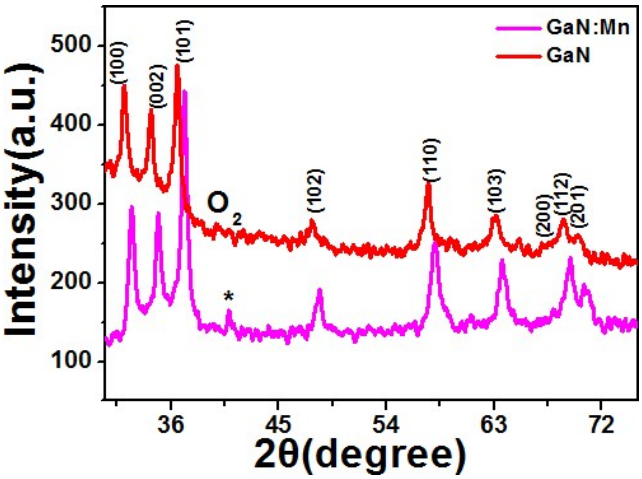

Fig. 1 XRD patterns of GaN and GaN:Mn nanoparticles. It shows the peak position of the GaN:Mn nanoparticles shifted slightly toward larger angle with the Mn addition.

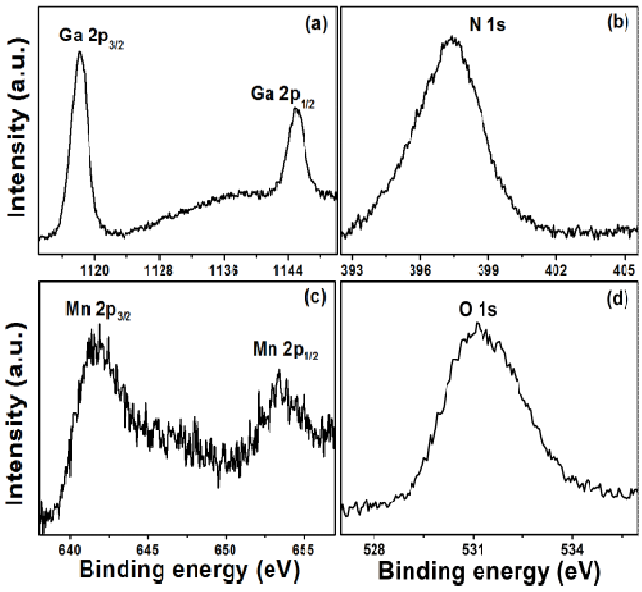

Fig. 2 XPS spectra of the GaN:Mn nanoparticles. The peaks of the core level of Ga 2p, N 1s, Mn 2p, O 1s are shown in the Fig. 2 (a-d), respectively.

The detailed information/composition of the GaN:Mn nanoparticles was further investigated by using XPS. As shown Fig. 2(a), the peaks of Ga $2p_{3/2}$ and Ga $2p_{1/2}$ are located at the binding energies of 1118.1 eV and 1145.0 eV. The core level of Ga has a positive shift comparing to the Ga $2p_{1/2}$ peaks from

elemental Ga.[37-39] The binding energy of N 1s is located at 397.4 eV and the full-width at half maximum is about 3.3 eV in the Fig. 2(b). The width and slight asymmetry of the N 1s peak could be due to the chemisorbed elemental N in the as-synthesized GaN.[37] The sites in binding energies of Ga and N confirms the bonding between Ga and N excluding the elemental Ga. Fig. 2(c) shows the peaks of Mn $2p_{3/2}$ and Mn $2p_{1/2}$ located at the binding energies of 641.7 eV and 653.4 eV. The peak of the nanoparticles appears in the lower energy region compared to that of MnO, due to the lower electronegativity of N. Therefore, the peaks would be expected to originate mainly from the Mn (II)-N bonding structures. This bonding energy of Mn $2p_{3/2}$ is higher level than that of metallic Mn, indicating rare Mn clusters.[30] The XPS spectra of the Mn 2p core levels indicate that Mn ions exist in the crystal structure after the substitution of the Ga sites. The O 1s peak centered at 531.2 eV is given in Fig. 2(d). The binding energy of chemisorbed O_2 on the surface has been observed in the region of 531.4 eV.[40] Therefore, the O 1s peak is attributed to chemisorbed O_2 in the Fig. 2(d). In short, the analysis of XPS spectra can match with the result of XRD pattern, and it is suggestted that the composition of the sample is GaN:Mn without other impurities.

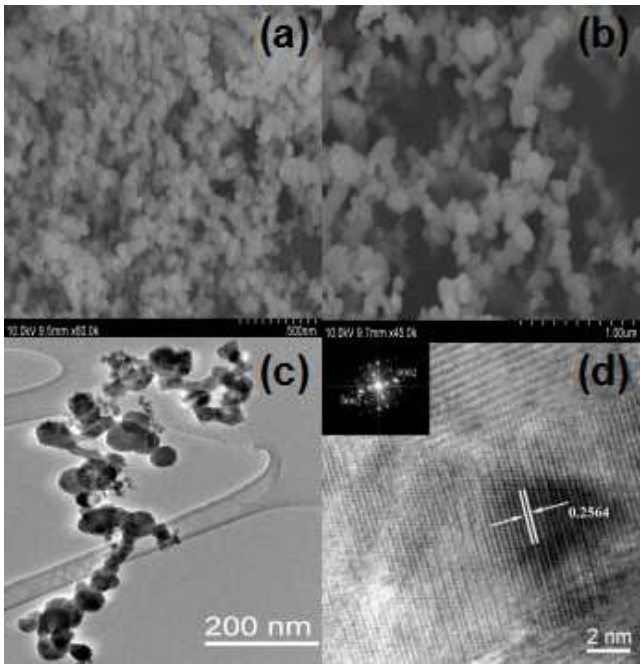

Fig. 3 the morphology images of GaN:Mn sample. (a) and (b) scanning electron microscopy (SEM) image. (c) transmission electron microscopy (TEM). (d) high-resolution transmission electron microscopy (HRTEM), the Fast Fourier transforms (FFT) of HRTEM images (insert in Fig. 3d).

The morphology and structural characterization of the GaN:Mn nanostructure are shown in Fig. 3. It is shown a scanning electron microscopy (SEM) image of typical GaN:Mn hexagonal nanoparticles about 8-70 nm in diameter in the Fig. 3a and 3b. The smaller particles exhibit almost spherically shaped corresponding to the initial state of the particle growth, and a prolonged treatment also lead to the formation of bigger hexagonal particles. The size of nanoparticles can be controlled by the reaction time; the samples prepared by a short treatment having significantly smaller size. Interestingly, the GaN:Mn nanoparticles are not independent, the GaN:Mn nanoparticles try to approach each other forming chains stacked by self-assembly (Fig. 3b). It is seemed as natural magnetic stacked together with each other.

The detailed microstructures characterization of the GaN:Mn nanoparticles was performed by transmission electron microscopy (TEM) and high-resolution transmission electron microscopy (HRTEM). The low resolution image displays the morphology of the prepared samples is mainly spherical in shape and stick together to form a chain, and the size varying from 8 nm to 70 nm. A representative HRTEM image of the GaN:Mn nanoparticles in the Fig. 3d. The Fast Fourier transforms (FFT) of HRTEM images (insert in Fig. 3d) corresponds to the X-ray diffraction pattern, and confirms the hexagonal structure of GaN:Mn. The spacing of 0.2564nm measured from the lattice fringe corresponds to the d-spacing of the (0002) plane. The d spacing obtained from HRTEM confirms the XRD data. To the best of our evidence, we can believe that we successfully prepared the GaN:Mn nanoparticles.

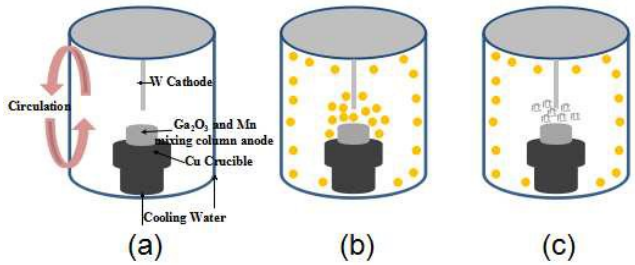

Fig. 4 the scheme of the growth of the GaN:Mn nanoparticles.

To explore the formation mechanism of the GaN:Mn nanostructures, it is essential to know the growth model. In this work, no metallic particle catalyst or template was used, the formation of the individual GaN:Mn nanoparticles should be related to the vapor-solid (VS) mechanism due to the intrinsic properties of GaN:Mn, such as the anisotropy of its hexagonal structure. Based on the above observation, the growth of the GaN:Mn nanostructures can be illustrated schematically in Fig. 4. As the processing temperature increases up to 3000-5000 ℃, the thermal decomposition of N_2 and NH_3 and the evaporation of Ga_2O_3 and Mn column result in the formation of Ga, Ga_2O, O_2, Mn, N, NH_2 and H_2 vapors, which are transported by N_2 carrier gas to a zone with an appropriate temperature for the growth GaN:Mn crystals through the following reaction: N + Ga +Mn→ GaN:Mn or $Ga_2O + NH_2 + Mn$→ GaN:Mn + H_2O +H_2. It is well known that the process of high-temperature nitriding reaction can obtain high quality GaN crystal without Ga_2O_3 and other phase of Ga, due to lattice defects and improvement of crystallization. During this step, the heat convection and temperature gradient produced by DC arc plasma provide a chemical-vapor transport and condensation process, which is responsible for the nucleation of GaN:Mn. On the basis of the above observations, we believe that the growth of GaN:Mn crystals could be a homogeneous nucleation process for the primary GaN:Mn nanoparticles formed at an early reaction stage. Then some crystal nucleus movement to the low temperature area with the circular flow, and in this area the slow evaporation of Ga, Ga_2O and Mn and a shortage of N and NH_2 vapors. The degree of supersaturation of GaN:Mn vapor decreases, and it is not enough to provide the growth of GaN:Mn microboxes forming spherically shaped particles. However, at the

higher temperature area the flashing evaporation of Ga, Ga_2O and Mn and enough of N and NH_2 vapors, and the energetic growth of GaN:Mn microboxes forms the bigger hexagonal particles. So the GaN:Mn nanoparticles are the inhomogeneity size, this phenomenon agrees with the morphological characterization.

Fig. 5 shows the PL spectrum of GaN:Mn nanoparticles excited using a frequency tripled Ti Sapphire laser as excitation source at room temperature. The excitation photon energy was set at 4.8 eV. The PL feature of GaN:Mn nanoparticles shows three broad emission bands centered at about 467 nm, 580 nm and 658 nm. According to the equation $E_v/eV=1240/\lambda$, the peaks corresponds to E_v= 2.65 eV, 2.13 eV, 1.88 eV, respectively. The spectrum of GaN:Mn shows a relatively broad range of visible light absorption. This is due to dopant-induced energy levels within the band gap increasing the yield for electron-hole pair formation under illumination with visible light. The peak at 467 nm (2.65 eV) is most likely due to transition from deep donorlike states due to the Mn dopant to the covalent band states; other emission peaks are also related to some impurity level. The doped is conducive to visible light absorption activity.[41] The intensive PL emission spectrum indicates that the existence of Mn in the structure influences the optical property.

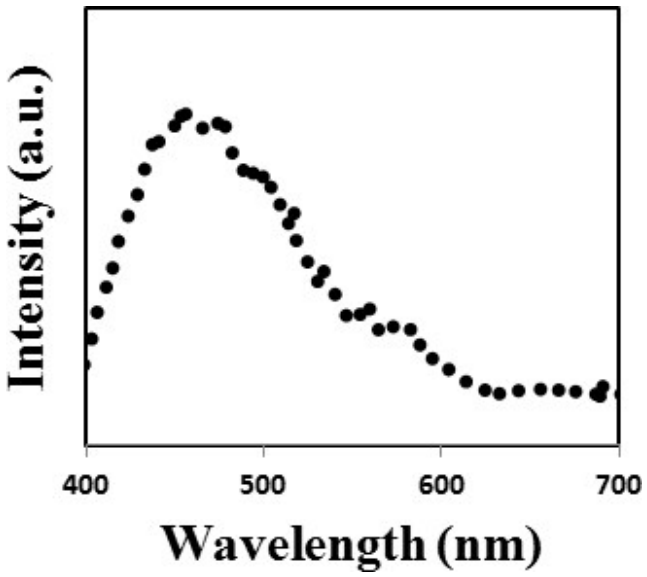

Fig. 5 Photoluminescence spectra (PL) of GaN:Mn nanoparticles using a frequency tripled Ti Sapphire laser as excitation source at room temperature.

In depth analysis of the magnetic properties is the central point of a DMS study. The magnetic measurements were performed at room temperature. In order to avoid getting false-positive magnetism signals due to high-sensitivity devices, it tested the undoped and Mn-doped GaN using the vibrating sample magnetometer (VSM). The Fig. 6a shows a hysteresis loop about the M-H curves of the pure GaN and GaN:Mn with different dopant concentration at 300 K. The undoped GaN nanoparticles show an almost zero hysteresis loop in Fig. 6a, implying the undoped GaN is non-magnetic. However, the M-H curves of the GaN:Mn nanoparticles show a hysteresis loop. The saturation magnetization of the GaN:Mn hexagonal nanoparticles are 0.013 $emug^{-1}$ and 0.016 $emug^{-1}$, and the coercive field are 103 Oe and 185 Oe for the samples with Mn concentrations of 4% and 7%, respectively. It is seen that the hysteresis loops are irreversible, while the irreversibility of the hysteresis loops are extremely small, indicating the presence of ferromagnetic or superparamagnetic-like which is the characteristic of the ferromagnetic particle with small size.[42] In addition, the saturation magnetization increases with increasing doped concentration. Since neither Ga^{3+} nor Mn^{2+} ions are magnetic ions, the observed magnetism is an intrinsic property of GaN:Mn and relate to the doped Mn ions.

To gain insight into the magnetic property for GaN:Mn nanoparticles, the temperature dependence of magnetization ZFC-FC curves were measured. Fig. 6b shows the zero-field-cooling (ZFC) and field-cooling (FC) curves of the GaN:Mn nanoparticles (7%) measured in a temperature range between 5 and 400 K at an applied magnetic field of 500 Oe. The Mn-doped GaN shows a distinct splitting between ZFC and FC measurement, implying the presence of a magnetic transition temperature. The ZFC magnetization increases as the temperature reduces from 400 K and reaches a maximum at 166 K, which is the phase transition point called the blocking temperature (T_B). The classically thermal-assisted superparamagnetic is blocked at the T_B, forwarding the phase transition from superparamagnetic state to magnetic long-range order.[11] The exponential decrease of the magnetization when increasing the temperature is a typical signature of superparamagnetic. Moreover, there is the existence of irreversibility between the FC and ZFC branches of the susceptibility below the T_B, presenting the typical behavior of superparamagnetic particles. The larger difference between ZFC and FC data indicates a large anisotropic field within the GaN:Mn nanoparticles.[43] The ZFC magnetization decreases from the T_B, but the magnetization starts increases when the temperature reduces to 70 K. This temperature is T_C, which is the renarkable transition point giving a clear-cut evidence of Quantum tunneling of magnetization (QTMs) from magnetic long-range order to QSP state in the GaN:Mn nanoparticles. This phenomenon is consistent with reports of such behavior at the nanoscale.[11, 42, 43] It is suggested that the dramatic increase in surface to volume ratio causes a stronger surface anisotropic field to frustrate and disorder the surface spin, which provides channels for quantum tunneling between spin-glass and quantum paramagnet, thus the quantum phase transition from magnetic long-range order to QSP state can be observed.[12]

The GaN:Mn nanoparticles possesses the complicated magnetism: the classical thermally driven from SP to blocked SP and the quantum phase transition from magnetic long-range order to QSP state. This phenomenon can be ascribed to the smaller size of GaN:Mn nanoparticles. The magnetic behavior is attributed to the Mn ions. A nonhomogeneous distribution of Mn favors the formation of Mn enriched and some isolated areas, the magnetic coupling between the Mn atoms depend on this distribution. The Mn-Mn and Mn-N distances are two important factors. The Mn-N distance may play a more crucial role than the Mn-Mn distance in dictating the magnetic coupling between the two Mn atoms.[44] The role of N mediates the magnetic coupling between Mn atoms. When the Mn-N distance exceeds some critical value, the magnetic coupling is ferromagnetic. Otherwise, the Mn-Mn (Mn-N) distances of the antiferromagnetic coupling are smaller than that of ferromagnetic coupling. Some theory studies show Mn atoms prefer to stay as close as possible to each other in the lattice.[45] When the high concentration of Mn in the GaN:Mn nanoparticles, the Mn-N distances of the ferromagnetic couping should be more. At the same time, the Mn-Mn (Mn-N) distances of the antiferromagnetic couping also be more. The accumulation of ferromagnetic and antiferromagnetic has determined the intensity of saturation magnetization. The superposition of result is that the sample shows ferromagnetism.

The increase of saturation magnetization is not proportional to the change of Mn content. Thus, Fig. 6a shows that the saturation magnetization of Mn content 7% is only bigger than that of Mn content 5%. In short, the magnetism of GaN:Mn is contributed by the Mn doped, the magnetic coupling between Mn atoms in GaN depends on the Mn-N –Mn distances.

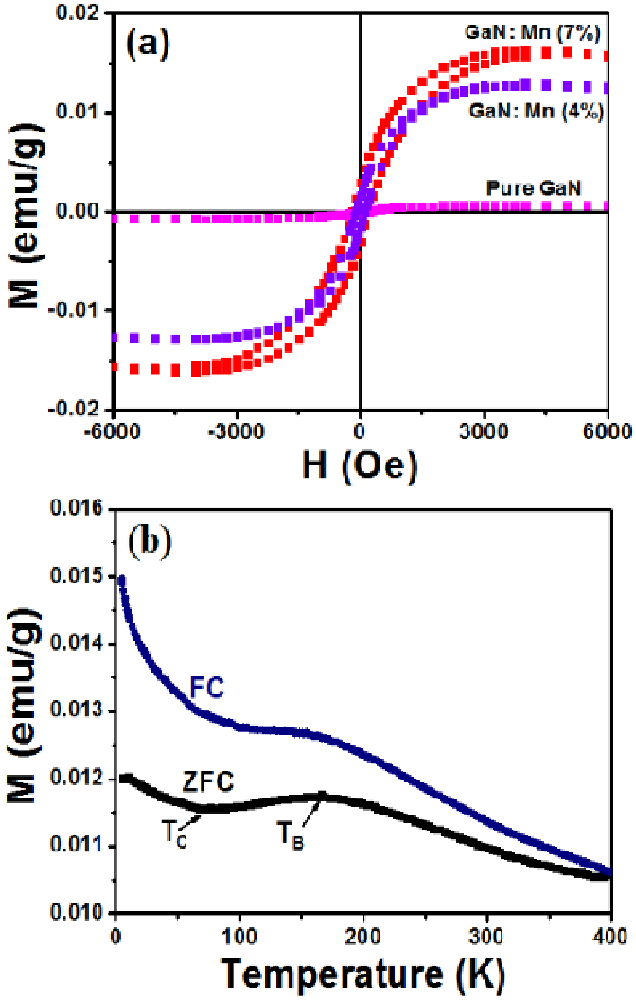

Fig. 6 (a) Magnetization hysteresis loop of the undoped and Mn doped GaN nanoparticles at room temperature. **(b)** ZFC and FC curves of the GaN:Mn nanoparticles.

Conclusions

In summary, a DC arc discharge plasma method synthesized the GaN:Mn nanoparticles of sizes about 8-70 nm have been developed. The Mn doped GaN nanoparticles have been studied structurally, morphologically by XRD, XPS, SEM, and HRTEM. The growth mechanism decides the characteristic of morphology and size. The intensive PL emission spectrum indicates that the existence of Mn in the structure and influencing the optical property. The complicated magnetic behavior of GaN:Mn nanoparticles has been testified via the experiment measurement, the classical thermally driven from SP to blocked SP and the quantum phase transition from magnetic long-range order to QSP state are observed in GaN:Mn nanoparticles. The magnetism is due to the Mn atoms, the magnetic coupling between Mn atoms in GaN depends on the Mn -Mn distances.

Acknowledgements

The authors thank Professor Yanzhang Ma and his team for technical support. This work was supported by the Education Department of Shaanxi Provincial Government Research Project (No. 14JK1131), the Dr. Scientific Research Foundation of Shaanxi University of Technology (SLGQD13(2)-11, SLGQD14-08), the National Science Foundation of China (No. 11074089, 51172087, NSAF. No:10976011) and the Open Subject of State Key Laboratory of Superhard Materials, Jilin University.

Notes and references

[a]*Institute of physics and telecommunications engineering, Shaanxi University of Technology, Hanzhong 723000, People's Republic of China. E-mail: appleyaobb@163.com.*

[b]*State Key Laboratory of Superhard Materials, Jilin University, Changchun, 130012, People's Republic of China. Fax: 86 0431 85166098; Tel: 86 0431 85166089; E-mail: cql@jlu.edu.cn.*

1. Y. Ohno, D. K. Young, B. Beschoten, F. Matsukura, H. Ohno and D. D. Awschalom, Nature, 1999, 402, 790.
2. H. Ohno, D. Chiba, F. Matsukura, T. Omiya, E. Abe, T. Dietl, Y. Ohno and K. Ohtani, Nature, 2000, 408, 944.
3. S. A. Wolf, D. D. Awschalom, R. A. Buhrman, J. M. Daughton, S. von Moln´ar, M. L. Roukes, A. Y. Chtchelkanova and D. M. Treger, Science, 2001, 294, 1488.
4. H. Ohno, Science, 1998, 281, 951.
5. W. W. Lei, D. Liu, Y. M. Ma, X. Chen, F. B. Tian, P. W. Zhu, X. H. Chen, Q. L. Cui and G. T. Zou, Angew. Chem. 2010, 122, 177.
6. J. Xu, J. Li, R. Zhang, X. Q. Xiu, D. Q. Lu, H. Q. Yu, S. L. Gu, B. Shen, Y. Shi, Y. D. Ye and Y. D. Zheng, Opt. Mater., 2003, 23, 163.
7. A. Neya, R. Rajarama, E. Arenholzc, J.S. Harris Jr., M. Samanta, R. F. C. Farrowa and S. S. P. Parkina, J. Magn. Magn. Mater., 2006, 300, 7.
8. D. D. Zhang, C. S. Xue, H. Z. Zhuang, H. B. Sun, Y. P. Cao, Y. L. Huang, Z. P. Wang and Y. Wang, ChemPhysChem., 2009, 10, 571.
9. S. Sapra, D. D. Sarma, S. Sanvito and N. A. Hill, Nano let. 2002, 2, 605.
10. K. Jayanti, S. Chawla, H. Chander and D. Haranath, Cryst. Res. Technol., 2007, 42, 976.
11. C. Xiao, J. J. Zhang, J. Xu, W. Tong, B. X. Cao, K. Li, B. C. Pan, H. B. Su and Y. Xie, Sci. Rep., 2012, 2, 755.
12. C. T. Hsieh and J. T. Lue, Phys. Lett. A, 2002, 300, 636.
13. Y. H. Deng, D. W. Qi, C. H. Deng, X. M. Zhang and D. Y. Zhao, J. Am. Chem. Soc., 2008, 130, 28.
14. J. Tejada, R. F. Ziolo and X. X. Zhang, Chem. Mater., 1996, 8, 1784.
15. S. C. Jain, M. Willander, J. Narayan and R. van Overstraeten, J. Appl. Phys., 2000, 87, 965.
16. T. Dietl, H. Ohno and F. Matsukura, Science, 2000, 287, 1019.
17. J. C. Johnson, H. J. Choi, K. P. Knutsen, R. D. Schaller, P. D. Yang and R. J. Saykally, Nat. Mater., 2002, 1, 106.
18. W. Q. Han, S. S. Fan, Q. Q. Li and Y. D. Hu, Science, 1997, 277, 1287.
19. W. Han, S. Fan, Q. Li and Y. Hu, Science, 1997, 277, 1287.
20. X. F. Duan and C. M. Lieber, J. Am. Chem. Soc. 2000, 122, 188.
21. L. W. Yin, M. S. Li, Y. Bando, D. Golberg, X. L. Yuan and T. Sekiguchi, Adv. Funct. Mater., 2007, 17, 270.
22. J. K. Yuan, W. Na. Li, S. Gomez and S. L. Suib, J. Am. Chem. Soc., 2005, 127, 14184.
23. M. Zajac, J. Gosk, E. Grzanka, S. Stelmakh, M. Palczewska, A.Wysmołek, K. Korona, M. Kami´nska and A. Twardowski, J. Alloys Compd., 2008, 456, 324.

24. M. C. Jeong, M. H. Ham, J. M. Myoung and S. K. Noh , App. Sur. Sci., 2004, 222, 322.
25. X. M. Cai, A. B. Djurisi, M. H. Xie, H. Liu, X. X. Zhang, J. J. Zhuc and H. Yang, Mat. Sci. & Eng. B, 2005, 117, 292.
26. G. Kunert, S. Dobkowska, T. Li, H. Reuther, C. Kruse, S. Figge, R. Jakiela, A. Bonanni, J. Grenzer, W. Stefanowicz, J. Von Borany, M. Sawicki, T. Dietl and D. Hommel, Appl. Phys. Lett., 2012, 101, 022413.
27. M. Zajaac, J. Gosk, M. Kaminska, A. Twardowski, T. Szyszko and S. Podsiadlo, Appl. Phys. Lett., 2001, 79, 2432.
28. Z. Ma, M. E. Jamer, E. Panaitescu, D. Heiman and L. Menon, J. Magn. Magn. Mater., 2015, 394, 155.
29. P. Simek, D. Sedmidubsky, S. Huber, K, Klimova, M. Marysko, M. Mikulics and Z. Sofer, Mater. Chem. Phys., 2015, 164, 108.
30. X. G. Cui and J. Zhang, Opt. Mater., 2015, 46, 299.
31. C. J. rawn and J. Chaudhuri, Advances in X-ray Analysis, 2000, 43, 338.
32. G. Thaler, R. Frazier, B. Gila, J. Stapleton, M. Davidson, C. R. Abernathy, S. J. Pearton and C. Segre, Appl. Phys. Lett., 2004, 84, 1314.
33. W. W. Lei, D. Liu, X. Chen and P. W. Zhu, J. Phys. Chem. C, 2010, 114, 15574.
34. Y. X. Jin, Q. L. Cui, G. H. Wen, Q. S. Wang and J. Hao, J. Phys. D: Appl. Phys., 2009, 42, 215007.
35. T. T. Hu, M. Z. Zhang, S. D. Wang and Q. J. Shi, CrystEngComm, 2011, 13, 5646
36. B. Matthias, M. H. Erie and D. Ulrike, Phys. Rev. Lett., 2006, 96, 026103.
37. E. Nahlah, R. S. Srinivasa and S. Major, Thin Solid Films, 1998, 333, 9.
38. C. R. Kingsley, T. J. Whitaker and A. T. S. Wee, Mater. Sci. Eng. B, 1995, 29, 78.
39. T. Sasaki and J. Matsuoka, Appl. Phys., 1998, 64, 4531.
40. F. M. Amanullah, K. J. Pratap and V. B. Hari, Mater. Sci. Eng. B, 1998, 52, 93.
41. B. B. Yao, R. Zhao, S. Y. Lu, P. Wang and M. Z. Zhang, RSC Adv., 2013, 3, 138. .
42. B. B. Yao, P. Wang, S. M. Wang and M. Z. Zhang, Cryst. Eng. Comm., 2014, 16, 2584.
43. W. W. Zheng, P. Kumar, A. Washington, Z. X. Wang, N. S. Dalal, G. F. Strouse and K. Singh, J. Am. Chem. Soc., 2012, 134, 2172.
44. Q. Wang, Q. Sun and P. Jena, Phys. Rev. Lett., 2005, 95, 167202.
45. J. Kang and K. J. Chang, Phys. Rev. B, 2005, 71, 144409.